Towards High-Performing Paraffin-based Fuels Exploiting the Armored Grain Concept

Riccardo Bisin[⋆†]*, Christian Paravan*[⋆]*, Alberto Verga*[⋆] *and Luciano Galfetti*[⋆]
[⋆]*Politecnico di Milano, Aerospace Science and Technology Dept.,*
Space Propulsion Laboratory (SPLab)
34, via LaMasa, 20156, Milan, Italy
riccardo.bisin@polimi.it · christian.paravan@polimi.it · alberto.verga@polimi.it · luciano.galfetti@polimi.it
[†]Corresponding author

Abstract

The attractive features of hybrid rocket propulsion could be fully exploited, and the inherent drawbacks overcome thanks to the armored grain approach. The armored grain, a heterogeneous paraffin-based fuel grain consisting of a paraffin matrix embedding a 3D printed polymeric gyroid-like reinforcement, is studied inspecting the mechanical properties at compression and the ballistic response. Different armored grains are developed by (i) changing the formulation of the paraffin matrix and (ii) embedding two different gyroids. The proper tailoring of the two constituents of the armored grains, i.e., the reinforcement and the paraffin matrix, enables the development of fuels with enhanced mechanical and ballistic properties. The armored grain approach is effective in overcoming the brittleness of the paraffin fuels and in boosting their regression rates.

1. Introduction

In the recent years, hybrid rocket engines (HREs) for aerospace applications have received growing attention as testified by the study of these systems for different propulsive missions. NASA has considered a paraffin-based HRE for the Mars Ascent Vehicle (MAV); Virgin Galactic has conceived SpaceShipTwo, a N2O/Polyamide hybrid motor for space tourism; Gilmour Space Technologies, HyImpulse Technologies GmbH, TiSPACE are some new players in the space industry that are developing launch systems based on HREs. The potential of HREs can be fully exploited by using paraffin-based fuels since they are affordable, low-toxic and they offer faster regression rates than traditional polymeric fuels [1, 2]. However, the intrinsic brittleness of paraffin fuels prevents their implementation in real flying systems. Hence, the mechanical properties of paraffin waxes need to be enhanced. Traditionally, this is pursued by blending paraffins with thermoplastic polymers [3, 4, 5, 6, 7, 8]. This approach can significantly improve the elasticity and the strength of the fuel grain. However, this method implies increased viscosity of the melted fuel, lowering the entrainment capability and consequently the fuel regression rate [6, 9].

In this framework, the Space Propulsion Laboratory (SPLab) of Politecnico di Milano is investigating different strategies to enhance the structural behavior of paraffin-based fuels without reducing the ballistic response [10]. In the recent years, the armored grain concept has been proposed as an alternative to blending paraffin waxes with polymers [11]. In this strategy, a 3D printed structure ('the reinforcement', 'the armor') is embedded in the paraffin fuel grain ('the paraffin matrix') to provide structural enhancement, as shown in Fig. 1. This new heterogeneous fuel is named *armored grain*. The previous researches investigated the effect of different polymers (polylactic acid, acrylonitrile butadiene styrene, nylon) [12, 13] and different geometries (the gyroid, the Schwarz Primitive, and both straight and twisted honeycombs) for the inner armor [14].

This work focuses on the the paraffin matrix and its impact on the structural and ballistic behavior of the armored grains. Different paraffin formulations are considered as surrounding matrix for the 3D printed reinforcement. These are presented in the unblended form (pristine wax) and in the blended form with 5% and 10% mass fractions of SEBS-MA (styrene-ethylene-butylene-styrene copolymer grafted with maleic anhydride) as the straightening agent. Gyroids at 10% and 15% volume fractions (aka infills) are considered as the 3D printed reinforcements to inspect the effect of different structures (same topology, but different volumes) on the characteristics of the armored grain. The acrylonitrile butadiene styrene (ABS) is selected as the 3D printer polymer for the gyroid production. The final purpose is to find the configuration that provides the best trade off in terms of mechanical and ballistic properties. To this end, mechanical tests at compression and static firings are carried out.

2. The Armored Grain

In the last years the armored grain has been proposed as a possible solution to the long-standing problem of enhancing the mechanical properties of paraffin-based fuels without reducing the ballistic behavior. The final goal is making the hybrid rocket technology based on paraffin fuels an effective and actual solution for different aerospace applications. The rationale of the armored grain, which is illustrated in Fig. 1, was creating a solid fuel with a fast-burning behavior and enhanced structural characteristics. To this end, the paraffin fuel was not doped with reinforcing thermoplastic polymers, whose presence in the fuel increases the viscosity and lowers the ballistic response. On the contrary, the structural improvement was pursued by embedding a 3D printed reinforcement (aka scaffold, armor).

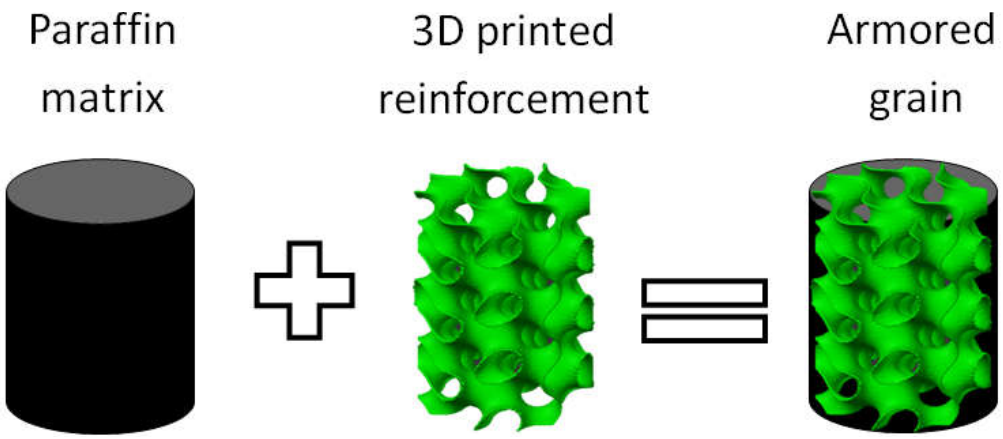

Figure 1: Armored grain concept exploiting 3D printed gyroid reinforcement [14].

The armored grain has its origin in the success of additive manufacturing and in a previous work of Galfetti et al. [15], where a poly-urethane foam (PUF) was used as a strengthening structure for the paraffin matrix. The advent of additive manufacturing offered endless possibilities, which were also seized by the hybrid rocket technology [16]. The availability of different polymeric materials fostered the use of 3D printing to produce cylindrical solid fuels with standard [17, 18] or complex geometries [19, 20], and axial-injection end-burning grains [21]. This technology was also used to 3D print structures to carry a high performing fuel, such as the paraffin wax. Studies were conducted on porous ABS structures impregnated with paraffin wax [22], and on acrylic honeycombs [23].

In the wake of these studies, the armored grain concept was conceived and proposed at the 8th European Conference for Aeronautical and Space Sciences (EUCASS) [12, 13]. The first investigation involved armored grains consisting of a micro-crystalline wax (Sasol0907) and of a cellular structure, the gyroid, as the inner reinforcement. The gyroid was produced in polylactic acid (PLA), acrylonitrile butadiene styrene (ABS), and nylon 6 (NY) and it represented the 15% by volume of the entire fuel. The pre-burning behaviors of the raw polymers were tested by evaluating the thermal properties (thermogravimetric analysis and differential scanning calorimetry), the critical surface tensions and the surface free energies [12, 24]. The mechanical properties at compression of the gyroids and the corresponding armored grains were measured. The test campaign revealed that the presence of the gyroid overcomes the brittleness of the pristine paraffin wax. Surprisingly, the fast-burning behavior of the paraffin wax was preserved, despite the presence of the gyroid made of slow burning materials [13]. The research on armored grains continued exploring different geometries for the armor: Schwarz Primitive, gyroid, traditional honeycombs and honeycombs with swept channels [14]. The different behavior at compression of the geometries directly affected the structural response of the armored grains. Although the armored grains based on Schwarz Primitive and on the gyroid offered the highest regression rates, all the fuels presented similar ballistic performance. These studies showed that the mechanical and ballistic behaviors of armored grains can be modified by changing the inner reinforcement, especially the polymer [12, 13, 24] and the topology [14]. The present work focuses on the other constituent of the armored grain: the paraffin matrix. To this aim, different paraffin formulations in the unblended and blended forms are considered. Two gyroids in ABS with different infills are also exploited for the armor.

In recent years, other research groups have started studies about paraffin-based fuels reinforced by different 3D printed structures: PLA gyroids [25, 26], nylon-12 scaffolds [27, 28], ABS helical structures and skeletons [29, 30], and spiral aluminum frameworks [31].

3. Investigated Materials and Fuels

In the present study, the fuels can be classified in two families: paraffin-based formulations and armored grains. The former group includes two pure waxes and their SEBS-MA blends. These fuels are combined with two different 3D printed gyroid in ABS (GY_15, GY_10) to obtain the armored grains. The fuels tested at compression are cylindrical grains with 30 mm diameter, 50 mm length. The specimens for ballistic tests feature the same dimensions and a 5 mm central port perforation.

3.1 Paraffin-Based Fuels

The paraffin-based fuels considered in the present work are listed in Table 1. The fuels are based on two paraffin waxes: a micro-crystalline wax (W1) and a macro-crystalline one (J1). All the fuels contain 1 wt% of carbon black as opacifier. Paraffin blends were also produced by doping the two pristine waxes with 5% and 10% mass fractions of SEBS-MA to improve the mechanical proprieties. The six fuels reported in Table 1 were also used as the paraffin matrices for the armored grains in Sec.3.2. All the specimens are produced via melt-casting approach: the pristine wax is heated above the melting temperature, the SEBS-MA is added and mixed (if needed), the compound is poured inside the specific mold. Concerning the specimens for the firing tests, a 5 mm hole is drilled in fuel.

Table 1: Investigated paraffin-based fuel formulations.

Fuel	**Mass fraction, [%]**				**TMD,**
	SasolWax 0907	**Macro-crystalline Wax**	**SEBS-MA**	**CB**	ρ_f [g/cm^3]
W1	99	0	0	1	0.929
W1S05	94	0	5	1	0.928
W1S10	89	0	10	1	0.928
J1	0	99	0	1	0.915
J1S05	0	94	5	1	0.915
J1S10	0	89	10	1	0.915

3.2 Armored Grains

The armored grains considered in the present work are listed in Table 2. Three different groups can be identified depending on the pristine paraffin wax (W1 or J1) and the gyroid reinforcement (GY_15 and GY_10) used for the armored grains. The specimens are named after the two main ingredients: the paraffin matrix (refer to Table 1) and the embedded gyroid structure (GY_15 and GY_10). Concerning the paraffin matrix, the W1 and the J1 waxes were used in both the pristine and SEBS-MA-blended form. Regarding the reinforcement, two gyroids were 3D printed in ABS: the GY_15 and GY_10. The former presents $\approx$ 15% volume fraction (infill) and it is manufactured following the *SPLab gyroid* design process [24]. The latter features $\approx$ 10% volume fraction and it is created according to the *infill gyroid* design process [24]. The main attribute differentiating the two gyroids is the different volume fraction (volume of the gyroid divided by the enveloped volume of the entire grain). The armored grains are produced via melt-casting approach: the 3D printed gyroid is lodged in a cylindrical mold, where the melted paraffin formulation (refer to Table 1) is poured.

The specimens in Table 2 provide an insight in the main features characterizing the armored grains. The influence of the paraffin fuel matrix is investigated contrasting the XX_GY_15 samples, which are composed by different pristine waxes (W1 and J1) and different amount of SEBS-MA (0%, 5%, 10%). Comparing the W1XX_GY_15 and the W1XX_GY_10 samples, it is possible to inspect the role of the reinforcement.

4. Methodology

The investigation of the armored grains was pursued by studying the mechanical response at compression and the ballistic performance via static firing tests. The W1 and its blends were also tested.

Table 2: Investigated armored grains (paraffin wax matrix + 3D printed ABS gyroid reinforcement). The compositions are expressed as percentage by volume (infill).

Fuel	**Volume fraction, [%]**								**TMD**
	Paraffin matrix						**ABS gyroid reinforcement**		ρ_f [g/cm^3]
	W1	**W1S05**	**W1S10**	**J1**	**J1S05**	**J1S10**	**GY_15**	**GY_10**	
W1_GY_15	85	-	-	-	-	-	15	-	0.947
W1S05_GY_15	-	85	-	-	-	-	15	-	0.947
W1S10_GY_15	-	-	85	-	-	-	15	-	0.947
J1_GY_15	-	-	-	85	-	-	15	-	0.932
J1S05_GY_15	-	-	-	-	85	-	15	-	0.935
J1S10_GY_15	-	-	-	-	-	85	15	-	0.936
W1_GY_10	90	-	-	-	-	-	-	10	0.943
W1S05_GY_10	-	90	-	-	-	-	-	10	0.943
W1S10_GY_10	-	-	90	-	-	-	-	10	0.942

4.1 Mechanical Characterization: Compression Tests

The structural assessments of the paraffin-based formulations (W1 and its blends, Table 1), the 3D printed structures (GY_15, GY_10) and the armored grains (Table 2) were carried out by means of uniaxial compression tests according to the ISO 604 [32]. Specimens under compression are shown in Fig. 2. An MTS 810 universal testing machine with a 250 kN load cell was used. The compression tests were conducted at ambient temperature (22 ± 3°C) with compression rate of 1 mm/min. Four samples were tested per each type of specimen. The test campaign provided the stress-strain relationship for the different fuels and the mechanical properties at compression, such as the Young modulus (E), the yield point, in terms of yield stress (σ_y) and yield strain (ϵ_y).

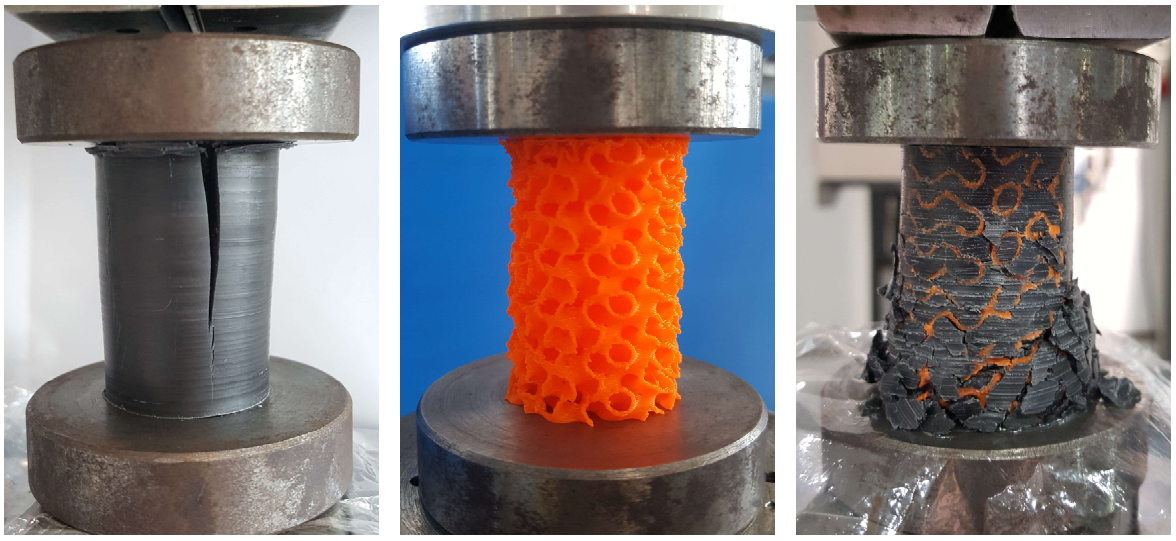

(a) Paraffin fuel: W1S10. (b) Gyroid reinforcement: GY_15. (c) Armored grain: W1S10_GY_15.

Figure 2: Investigated materials during compression tests.

4.2 Ballistic Characterization: Firing Tests

The ballistic characterization of the fuel grains was assessed via static firing tests aiming at measuring the regression rate (r_f). Tests were carried out at the SPLab in lab-scale hybrid rocket motor, which is sketched in Fig. 3. The facility is designed to burn single-port, center-perforated cylindrical grains. Samples for the firing tests feature the same geometry and size of the ones for the compression tests (Sec. 4.1), with the only difference of an initial central port of 5 mm diameter.

The motor consists of an injector head, a pre-combustion chamber where the pyrotechnic igniter is placed, a combustion chamber lodging the fuel grain, a post-combustion chamber, and a water-cooled brass nozzle. The injector head is equipped with a quartz window for recording the combustion with a high-speed camera.

Firing tests were performed with gaseous oxygen (GOX) as oxidizer. For each type of fuel, at least three tests were carried out under the same operating conditions. The shutdown of the motor was accomplished by interrupting the GOX flow (closure of the OX electrovalves) and by injecting gaseous N2 (opening of the N2 electrovalves) in the combustion chamber to quench the flame and purge the system. The GOX mass flow rate was controlled by a digital flowmeter and kept constant at 5 g/s for the test duration, corresponding to an initial oxidizer mass flux (G_{ox}) of $\approx$ 250 kg/(m^{2}s). The combustion duration (firing time) $\Delta t_b = t_{end} - t_{in}$ was retrieved by analyzing the recorded pressure trace. The t_{in} is the time at which the chamber pressure starts raising. The t_{end} is the time at which the gaseous nitrogen is injected into the combustion chamber to quench the combustion. The Δt_b was chosen according to the fuel formulation to obtain approximately the same final diameter, thus the same average $\bar{G}_{ox}$, for all the tested grains. In fact, the oxidizer mass flux is the most significant parameter affecting the r_f [33, 2], so having approximately the same $\bar{G}_{ox}$ for all the samples was preferred instead of maintaining a fixed Δt_b. The burning time spanned from 4 s, for the fastest formulations (i.e., W1_GY_10), to 14 s, for the slowest one (i.e., 3D printed ABS).

The space-time average regression rate of the solid fuel r_f is calculated as the variation of the port diameter occurred during the firing [2]:

$$r_f = \frac{1}{\Delta t_b} \frac{D(t_{end}) - D(t_{in})}{2} \tag{1}$$

The final port diameter $D(t_{end})$ is evaluated by measuring the fuel mass variation Δm_f (weight of the fuel checked before and after the firing):

$$D(t_{end}) = \sqrt{D(t_{in}) + \frac{4}{\pi} \frac{\Delta m_f}{\rho_f \cdot L_f}} \tag{2}$$

where ρ_f and L_f are the density (refer to Tables 1 and 2) and the initial length (i.e., 50 mm) of the fuel grain, respectively. The average oxidizer mass flux ($\bar{G}_{ox}$) of the test can be estimated dividing the oxidizer mass flow rate ($\dot{m}_{ox} = 5\, g/s$) by the average port area:

$$\bar{G}_{ox} = \frac{16 \cdot \dot{m}_{ox}}{\pi \cdot [D(t_{end}) + D(t_{in})]^2} \tag{3}$$

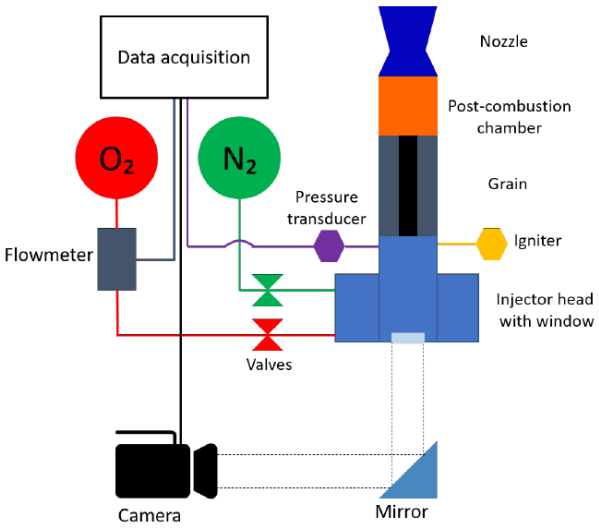

Figure 3: Schematics of the SPLab lab-scale hybrid rocket motor [13].

5. Results

5.1 Compression Tests Results

The mechanical responses at compression of the W1-based fuels and of the armored grains are illustrated in Fig. 4 in terms of (average) stress-strain curves. The mechanical properties are listed in Table 3, where the Young modulus (E) and the yield point are reported (σ_y and ϵ_y).

Table 3: Mechanical properties at compression of all the investigated materials: W1 paraffin-based formulations, gyroid structures, armored grains (compression rate 1 mm/min, testing temperature 22 ± 3°C) [34]. Ensemble average values derived by four runs for each sample.

Specimen	**Young modulus**, E [MPa]	**Yield stress**, σ_y [MPa]	**Yield strain**, ϵ_y [%]
W1	407	3.46	1.47
W1S05	390	3.75	1.71
W1S10	510	4.92	1.86
GY_15	26	1.14	8.07
GY_10	16	0.46	6.59
W1_GY_15	205	2.71	5.33
W1S05_GY_15	265	3.02	3.80
W1S10_GY_15	352	4.19	3.50
W1_GY_10	171	2.42	≈15
W1S05_GY_10	329	3.27	1.58
W1S10_GY_10	396	4.25	1.85
J1_GY_15	195	2.33	3.95
J1S05_GY_15	296	3.40	4.32
J1S10_GY_15	350	4.94	3.94

The brittle behavior of the W1-based paraffin fuels is shown in Fig. 4a, where the $\sigma(\epsilon)$ curves exhibit a drop after the yield point (maximum stress), which also coincides with the failure point. In fact, the paraffin formulations are stiff (high E values in Table 3) and brittle (low ϵ_y in Table 3) with a deformation process involving cracks and a frail rupture, as illustrated in Fig. 2a. The presence of SEBS-MA in the W1 strengthens the pure wax, enhancing the σ_y by 8% and by 42% when using 5 wt% and 10 wt% of SEBS-MA, respectively. The yield strain is also increased, but the rupture still occurs below 2% of strain. The effect of SEBS-MA on the Young modulus is not straightforward since the E of the W1 wax is between the one of W1S10 and of W1S05.

Table 3 and Figs. 4b- 4d display the mechanical behaviors of the gyroids (GY_15 and GY_10). Their compressive properties (E and σ_y in Table 3) are significantly lower than the ones of the W1-based formulations. The specimens experience a plateau stress after the yield point and the GY_15 exhibit a stronger (higher σ_y) and stiffer (higher E) behavior than the GY_10, which is the lightest reinforcement. This is in agreement with studies on foams and lattices, where scaling laws indicates that the relative density (i.e. the volume fraction) has a major impact on the mechanical properties of the structures [35].

Concerning the armored grains in Figs. 4b and 4c, the presence of a gyroid-like reinforcement is able to provide the brittle W1-based formulations with a ductile behavior. In fact, the armored grains feature an almost constant plateau stress after the yield point, unlike the W1 formulations. The inner armor confines the paraffin wax matrix avoiding the propagation of cracks (see Fig. 2c). In turn, the paraffin matrix acts as a filler for the gyroid. The armored grains exhibit a higher deformation energy (area below the stress-strain curve) than the 'not armored' fuel counterparts (W1-based formulations), suggesting the capability of armored grains to withstand high deformations and absorb energy. Comparing armored grains in Figs.4b and 4c, the effect of the reinforcement on the mechanical behavior can be appreciated. In fact, the armored grains present the same W1-based (unlbended and blended) formulations, but embedding different gyroids (GY_15 and GY_10). The W1_GY_15 manifests a stiffer and stronger behavior than the W1_GY_10, and this is consistent with the better mechanical properties of GY_15 than GY_10. On the contrary, the armored grains based on the SEBS-MA blends reverse this trend, with the W1S05_GY_10 and W1S10_GY_10 performing better than the W1S05_GY_15 and W1S10_GY_15. Even though the GY_15 behaves better at compression than the GY_10, the higher surface and volume fraction of the former could be detrimental for the mechanical properties of the armored grains. In fact, the gyroid-paraffin interface could be the location for the crack onset and the detachment of paraffin chunks from the inner armor. The higher volume fraction of the gyroid implies greater contact area between gyroid and paraffin, hence a potentially higher separation area.

The impact of the paraffin matrix on armored grains has been also studied by substituting the pristine wax: the micro-crystalline W1 wax was replaced with the macro-crystalline J1 wax, as shown in Figs. 4b and Fig. 4d. The poor mechanical behavior of the macro-crystalline J1 wax [34] results in lower stiffness and strength (Table 3) of the J1_GY_15 with respect to the W1_GY_15. The structural benefit of the presence of the SEBS-MA in the paraffin

matrix is evident for the J1-based armored grains (Fig. 4d) and it is more marked than for the W1-based ones (Figs. 4b). This could be related to the better mixing of SEBS-MA with J1 rather than with W1, hence to a good adhesion between the J1 blends and the ABS gyroid.

The three different families of the armored grains in Figs. 4b- 4d and Table 3 attest that blending the paraffin wax (W1 or J1) with SEBS-MA significantly enhances the mechanical properties of the fuels. The relative increments depends on both the crystalline nature of the pristine wax (J1 and W1) and on the inner armor (GY_15 and GY_10). The armored grains based on the W1 and the GY_15 (Fig. 4b) experience $\Delta\sigma_y$ of 11% and 55% when 5% and 10% of SEBS-MA is present in the paraffin matrix, respectively; armored grains based on the W1 and the GY_10 (Fig. 4c) are characterized by higher $\Delta\sigma_y$, around 35% and 76%; the most remarkable increments are achieved by armored grains based on the J1 and the GY_15 (Fig. 4d), whose $\Delta\sigma_y$ are 46% and 112%. Similar considerations hold for the Young modulus.

The experimental tests campaign highlights that the insertion of a gyroid does not increase the strength (σ_y) of the paraffin-based fuels. However, the armor is highly effective in enhancing the deformation energy, providing the fuel with a plastic field and making it capable of withstanding high deformations. Even though paraffin chunks and slivers detach from the inner gyroid, the entire armored grains do not crack in a frail way.

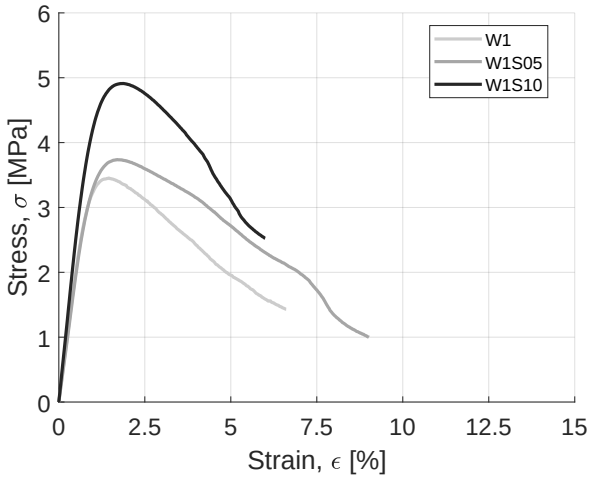

(a) Paraffin formulations: pure W1 and SEBS-MA blends.

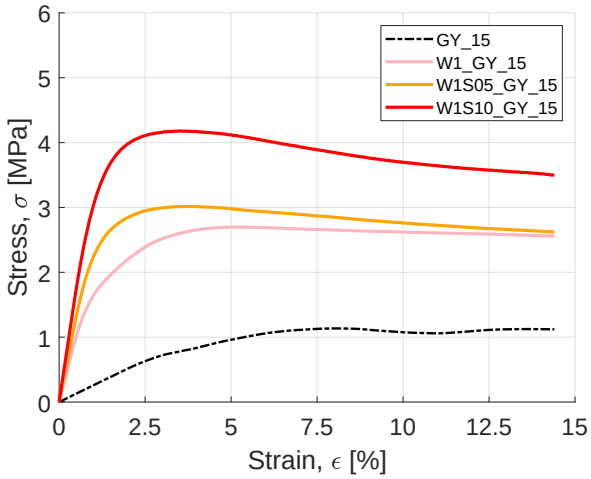

(b) Armored grains based on W1 formulations and GY_15 gyroid.

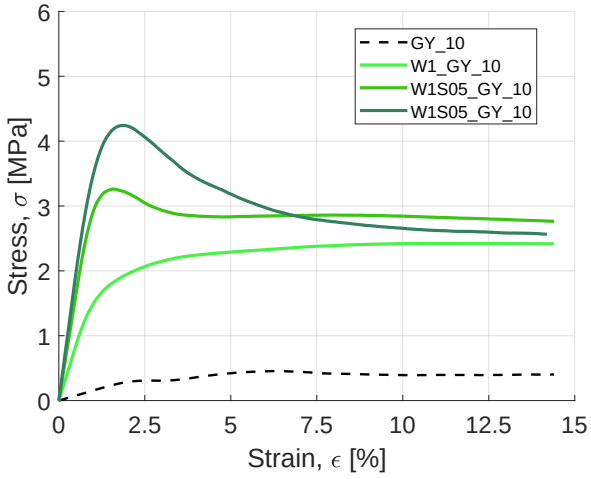

(c) Armored grains based on W1 formulations and GY_10 gyroid.

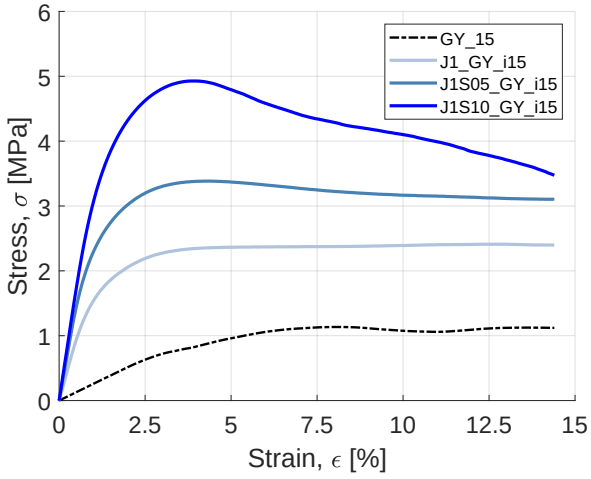

(d) Armored grains based on J1 formulations and GY_15 gyroid.

Figure 4: Engineering stress-strain curves at compression of the investigated fuels: (a) W1 paraffin-based formulations, (b-d) armored grains (ensemble average curves derived by four runs for each sample, compression rate 1 mm/min, testing temperature 22 ± 3°C). In Fig.(b-d) the dashed lines represent the mechanical behaviors of the gyroids GY_15 and GY_10.

5.2 Regression Rate Results

The results of the static firing tests are summarized in Table 4, where the average r_f of the different formulations are listed. Figure 5 illustrates the specimens after the firing tests. The 3D printed ABS fuel was also tested to provide a reference value of a polymeric fuel not undergoing entrainment. The closeness of the $\bar{G}_{ox}$ values allows the comparison of the ballistic performance under approximately the same operating conditions.

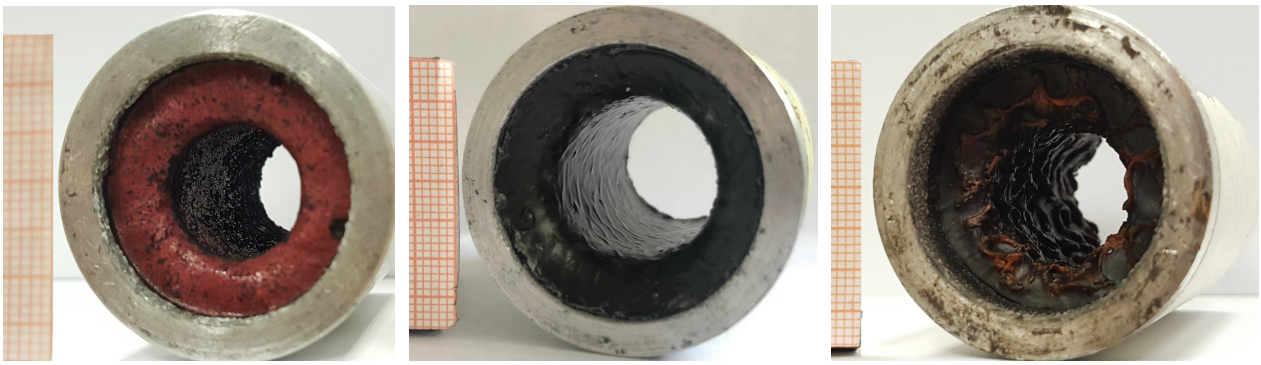

(a) 3D printed ABS. (b) Paraffin fuel: W1. (c) Armored grain: W1S10_GY_15.

Figure 5: Fuel samples after the firing tests. The oxidizer flow is direct inwards [34].

The fast-burning behavior of the paraffin waxes is testified contrasting the r_f values of the W1-based fuels with the one of the ABS. The values of the W1-based formulations are 1.7- to 2.6-fold higher than the r_f of the ABS. The amount of SEBS-MA in the W1 wax lessens the ballistic performance of the pristine wax, reducing the r_f by 22% and by 33% when 5% and 10% of SEBS-MA are present, respectively. This is due to the enhanced viscosity of the fuels because of the SEBS-MA [10].

The insertion of a 3D printed gyroid (GY_15 and GY_10) in the paraffin formulations does not reduce the r_f, although the bulk material of the gyroid (i.e. the ABS) is a slow burning material. In fact, the armored grains based on the W1 formulations and the GY_15 (W1XX_GY_15 series) feature r_f increments in the 43-55% range with respect to the not armored counterparts (compare W1_GY_15 with W1, W1S05_GY_15 with W1S05, and W1S10_GY_15 with W1S10). Moving to the armored grains based on the GY_10 (W1XX_GY_10 series), higher increments are observed, spanning from 75% to 91%. Hence, the presence of an inner armor boosts the ballistic performance of the paraffin formulations, and this enhancement is greater when embedding the lightest gyroid, the GY_10.

The replacement of the W1 with the J1 brings to an increment of the r_f, when the armored grains based on the unblended formulations are considered: the r_f of the W1_GY_15 is 1.75 mm/s, whereas the r_f of the J1_GY_15 is 2.08 mm/s (+19%). Negligible differences are observed for armored grain featuring SEBS-MA blends. The r_f of the W1S05_GY_15 is close to the one of the J1S05_GY_15. The same holds for the W1S10_GY_15 and J1S10_GY_15, whose r_f values (1.16 mm/s and 1.18 mm/s) are nearly the same of the pure W1 wax (1.21 mm/s).

The values in Table 4 clearly highlight the negative impact of SEBS-MA on all the investigated fuels. The increment of the melted fuel viscosity due to the SEBS-MA addition is not limited to the paraffin-based fuels, but it plays an important role also for the armored grains. In fact, the same r_f trend of paraffin-based fuels is also experienced by the armored grains. The r_f of the W1_GY_15 is reduced by 16% and 34% when adding 5% and 10% of SEBS-MA, respectively (refer to W1S05_GY_15 and W1S10_GY_15 samples). Similarly, the r_f of the W1_GY_10 is reduced by 19% (W1S05_GY_10) and 36% (W1S10_GY_10), and the r_f of the J1_GY_15 by 32% (J1S05_GY_15) and 43% (J1S10_GY_15).

The firing tests campaign attests that the insertion of a 3D printed gyroid does not lower the regression rate of the paraffin fuel, which is boosted instead. This could be related to the enhanced turbulence level inside the combustion chamber promoted by inner armor during the combustion. Armored grains exhibit rough and uneven burning surface (Fig. 5c), unlike the paraffin-based formulations (Fig. 5b) and the polymeric fuels (Fig. 5a). This feature indicates that the inner reinforcement burns together with the paraffin matrix and it could also raise the skin friction coefficient and the heat feedback to the fuel surface.

Table 4: Ballistic tests results of all the investigated fuels: ABS polymeric fuel, paraffin-based formulations and armored grains. Average values derived by three runs for each sample. Test conditions: initial fuel port diameter of 5 mm, oxidizer mass flow rate of 5 g/s.

Fuel	**Average oxidizer mass flux**, $\bar{G}_{ox}$ [kg/(m^{2}s)]	**Regression rate**, r_f [mm/s]
ABS	41 ± 4	0.47 ± 0.04
W1	36 ± 1	1.21 ± 0.04
W1S05	37 ± 4	0.95 ± 0.03
W1S10	40 ± 2	0.81 ± 0.03
W1_GY_15	33 ± 3	1.75 ± 0.06
W1S05_GY_15	32 ± 1	1.47 ± 0.07
W1S10_GY_15	39 ± 1	1.16 ± 0.02
W1_GY_10	29 ± 1	2.23 ± 0.13
W1S05_GY_10	32 ± 3	1.81 ± 0.21
W1S10_GY_10	36 ± 2	1.42 ± 0.10
J1_GY_15	30 ± 1	2.08 ± 0.05
J1S05_GY_15	35 ± 1	1.40 ± 0.06
J1S10_GY_15	39 ± 2	1.18 ± 0.04

6. Conclusion and Future Developments

The armored grain concept was investigated and explored to deepen the knowledge of this reinforcing strategy for paraffin-based fuels. The armored grain is a heterogeneous fuel composed by a 3D printed structure embedded in the surrounding paraffin matrix. In this work, the mechanical performance at compression and the ballistic response of armored grains and (unblended and SEBS-MA-blended) paraffin formulations were studied. The focus was inspecting the features that characterize the behavior of the armored grains. To this end, the two components of the armored grains were altered: the paraffin matrix was modified by adding SEBS-MA to the pure wax and by changing the pure wax itself; two ABS gyroids with different volume fractions were used for the inner armor.

The structural assessment via compression tests revealed that all the armored grains exhibit a plastic response overcoming the intrinsic brittleness of the paraffin-based formulations. The firing tests conducted in the lab-scale HRE with gaseous oxygen as oxidizer attested that the regression rates of both the unblended and blended paraffin formulations can be increased by embedding 3D printed reinforcement (i.e, in the armored grain configuration). The mechanical and ballistic characteristic of the armored grains were found to be dependent on (i) the paraffin matrix (presence of SEBS-MA and choice of the pristine wax), and (ii) the reinforcement (volume fraction of the gyroid).

Concerning the former aspect, the addition of SEBS-MA in the paraffin matrix enhances the strength (maximum allowable stress) and the stiffness (Young modulus) of the armored grains. The presence of 10% of SEBS-MA raised the strength of armored grains from 55 to 112%. This trend was also experienced by the paraffin-based fuels. Conversely, the SEBS-MA lessened the regression rate of armored grains, reducing the r_f by 34-43%. However, the 'slowest' armored grains, i.e., the ones having the 10% SEBS-MA in the paraffin matrix (W1S10_GY_15 and J1S10_GY_15), feature approximately the same r_f of the fastest paraffin formulation, i.e. the pure W1 wax. The replacement of the micro-crystalline W1 wax with the macro-crystalline J1 wax for the matrix of the armored grains (moving from W1_GY_15 to J1_GY_15) led to a slightly decrease of the strength at compression (-14%), but to an increment of the r_f (+19%). Concerning the reinforcement for the armored grain, the use of the GY_10 gyroid instead of the GY_15 produced limited σ_y and E variations, but r_f increments in the 22-27% range.

The concept of adding a 3D printed structure is effective in improving the mechanical properties of the paraffin fuels without ruining the ballistic response. The best trade off in terms of mechanical and ballistic properties could be achieved by combining the blending strategy with the armored grain concept. From this perspective, the armored grains featuring SEBS-MA in the paraffin matrix can be identified as the most promising configurations.

The results of the present work and the previous studies carried out at the SPLab of Politecnico di Milano make the armored grain a suitable answer for the long-standing research for green paraffin-based fuels featuring both structural and combustion performance. Future activities will be targeted at proving the feasibility of the armored grain for real flying systems. Larger-scale firing tests represent the next step.

References

[1] D. Altman, "Overview and history of hybrid rocket propulsion," in *Fundamentals of Hybrid Rocket Combustion and Propulsion* (M. J. Chiaverini and K. K. Kuo, eds.), ch. 1, pp. 1–36, AIAA, 2007.

[2] M. A. Karabeyoglu, G. Zilliac, B. J. Cantwell, S. DeZilwa, and P. Castellucci, "Scale-up tests of high regression rate paraffin-based hybrid rocket fuels," *J. Propul. Power*, vol. 20, no. 6, pp. 1037–1045, 2004.

[3] S. Kim, H. Moon, J. Kim, and J. Cho, "Evaluation of paraffin polyethylene blends as novel solid fuel for hybrid rockets," *J. Propul. Power*, vol. 31, no. 6, pp. 1750–1760, 2015.

[4] R. Kumar and P. A. Ramakrishna, "Studies on eva-based wax fuel for launch vehicle applications," *Propellants, Explos., Pyrotech.*, vol. 41, no. 2, pp. 295–303, 2016.

[5] M. Kobald, C. Schmierer, H. K. Ciezki, S. Schlechtriem, E. Toson, and L. T. De Luca, "Viscosity and regression rate of liquefying hybrid rocket fuels," *J. Propul. Power*, vol. 33, no. 5, pp. 1245–1251, 2017.

[6] C. Paravan, L. Galfetti, and F. Maggi, "A critical analysis of paraffin-based fuel formulations for hybrid rocket propulsion," in *53rd AIAA/SAE/ASEE Jt. Propuls. Conf.*, (Atlanta, GA), pp. 1–17, 2017.

[7] Y. Tang, S. Chen, W. Zhang, R. Shen, L. T. De Luca, and Y. Ye, "Mechanical modifications of paraffin-based fuels and the effects on combustion performance," *Propellants, Explos., Pyrotech.*, vol. 42, no. 11, pp. 1268–1277, 2017.

[8] Y. Matsumoto, K. Takahashi, K. Kinoshita, and K. Nakajima, "Characteristics of a polymeric as an additive in WAX-based hybrid rocket fuel," in *2018 Jt. Propuls. Conf.*, (Cincinnati, OH), pp. 1–9, 2018.

[9] K. Veale, S. Adali, J. Pitot, and M. Brooks, "A review of the performance and structural considerations of paraffin wax hybrid rocket fuels with additives," *Acta Astronaut.*, vol. 141, pp. 196–208, 2017.

[10] C. Paravan, L. Galfetti, R. Bisin, and F. Piscaglia, "Combustion processes in hybrid rockets," *Int. J. Energ. Mater. Chem. Propul.*, vol. 18, no. 3, pp. 255–286, 2019.

[11] R. Bisin, S. Alberti, A. Verga, C. Paravan, and L. Galfetti, "Green fuels for rocket propulsion: Current status and future perspectives of paraffin-based formulations," in *70th Int. Astronaut. Congr. (IAC)*, (Washington, DC), pp. 1–11, 2019.

[12] R. Bisin, C. Paravan, S. Alberti, and L. Galfetti, "An innovative strategy for paraffin-based fuels reinforcement: Part i, mechanical and pre-burning characterization," in *8th Eur. Conf. for Aeronaut. and Space Sci. (EUCASS)*, (Madrid, ES), pp. 1–14, 2019.

[13] R. Bisin, C. Paravan, A. Verga, and L. Galfetti, "An innovative strategy for paraffin-based fuels reinforcement: Part ii, ballistic characterization," in *8th Eur. Conf. for Aeronaut. and Space Sci. (EUCASS)*, (Madrid, ES), pp. 1–9, 2019.

[14] R. Bisin, C. Paravan, S. Parolini, and L. Galfetti, "Impact of 3D-printing on the mechanical reinforcement and the ballistic response of paraffin-based fuels: the armored grain," in *AIAA Propul. Energy 2020 Forum*, (Virtual Event), pp. 1–21, 2020.

[15] L. Galfetti, L. Merotto, M. Boiocchi, F. Maggi, and L. T. De Luca, "Ballistic and rheological characterization of paraffin-based fuels for hybrid rocket propulsion," in *47th AIAA/ASME/SAE/ASEE Jt. Propuls. Conf. Exhib.*, pp. 1–17, 2011.

[16] C. Oztan and V. Coverstone, "Utilization of additive manufacturing in hybrid rocket technology: A review," *Acta Astronaut.*, vol. 180, pp. 130–140, 2021.

[17] S. A. Whitmore, Z. W. Peterson, and S. D. Eilers, "Comparing hydroxyl terminated polybutadiene and acrylonitrile butadiene styrene as hybrid rocket fuels," *J. Propul. Power*, vol. 29, no. 3, pp. 582–592, 2013.

[18] M. McFarland and E. Antunes, "Small-scale static fire tests of 3D printing hybrid rocket fuel grains produced from different materials," *Aerosp.*, vol. 6, no. 7, p. 81, 2019.

[19] M. J. Degges, P. Taraschi, J. Syphers, D. Armold, J. E. Boyer, and K. Kuo, "Student investigation of rapid prototyping technology for hybrid rocket motor fuel grains," in *49th AIAA/ASME/SAE/ASEE Jt. Propuls. Conf.*, (San Jose, CA), pp. 1–12, 2013.

[20] S. A. Whitmore, S. D. Walker, D. P. Merkley, and M. Sobbi, "High regression rate hybrid rocket fuel grains with helical port structures," *J. Propul. Power*, vol. 31, no. 6, pp. 1727–1738, 2015.

[21] M. A. Hitt, "Preliminary additively manufactured axial-injection, end-burning hybrid rocket motor regression rate study," in *2018 Jt. Propuls. Conf.*, (Cincinnati, OH), pp. 1–5, 2018.

[22] J. McCulley, A. Bath, and S. A. Whitmore, "Design and testing of FDM manufactured paraffin-ABS hybrid rocket motors," in *48th AIAA/ASME/SAE/ASEE Jt. Propuls. Conf. Exhib.*, (Atlanta, GA), pp. 1–24, 2012.

[23] D. Armold, J. E. Boyer, K. Kuo, J. K. Fuller, J. Desain, and T. J. Curtiss, "Test of hybrid rocket fuel grains with swirl patterns fabricated using rapid prototyping technology," in *49th AIAA/ASME/SAE/ASEE Jt. Propuls. Conf.*, (San Jose, CA), pp. 1–14, 2013.

[24] R. Bisin, C. Paravan, S. Alberti, and L. Galfetti, "A new strategy for the reinforcement of paraffin-based fuels based on cellular structures: The armored grain – mechanical characterization," *Acta Astronaut.*, vol. 176, pp. 494–509, 2020.

[25] C. Hill, C. C. McDougall, T. Messinger, and C. T. Johansen, "Modification of paraffin-based hybrid rocket fuels using structural lattices," in *AIAA Propul. Energy 2019 Forum*, (Indianapolis, IN), pp. 1–10, 2019.

[26] C. Hill and C. T. Johansen, "Evaluation of lattice-augmented hybrid rocket fuels on a slab burner," in *AIAA Propul. Energy 2021 Forum*, (Virtual Event), pp. 1–12, 2021.

[27] D. Zdybal, W. Klos, P. Drozdz, Z. Rydz, K. Kobus, B. Wyciszkiewicz, A. Zwolak, M. Wyzlinski, T. Tatara, and A. Guzik, "Performance of solid state emulsions of isoamyl alcohol in eva-stabilized low-mw polyethylene, structured by laser-sintered nylon scaffolds as fuels in n2o hybrid rocket engine," in *AIAA Propul. Energy 2019 Forum*, (Indianapolis, IN), pp. 1–19, 2019.

[28] D. Zdybal, L. Pabarcius, A. Laczewski, B. Wyciszkiewicz, A. Zwolak, P. Slawecki, and M. Wyzlinski, "Investigation of fdm-printed open-framework-reinforced helical pewax grains as a robust, high regression hybrid rocket fuel," in *AIAA Scitech 2021 Forum*, (Virtual Event), p. 1247, 2019.

[29] Z. Wang, X. Lin, F. Li, and X. Yu, "Combustion performance of a novel hybrid rocket fuel grain with a nested helical structure," *Aerosp. Sci. Technol.*, vol. 97, p. 105613, 2020.

[30] Y. Wu, Z. Zhang, Q. Wang, and N. Wang, "Combustion characteristics of skeleton polymer reinforced paraffin-wax fuel grain for applications in hybrid rocket motors," *Combust. Flame*, vol. 241, p. 112055, 2022.

[31] X. Lin, D. Qu, X. Chen, Z. Wang, J. Luo, D. Meng, G. Liu, K. Zhang, F. Li, and X. Yu, "Three-dimensional printed metal-nested composite fuel grains with superior mechanical and combustion properties," *Virtual Phys. Prototyping*, vol. 17, no. 3, pp. 437–450, 2022.

[32] Int. Organ. Stand., "ISO 604:2002 Plastics - Determination of compressive properties." `https://www.iso.org/standard/31261.html`.

[33] T. Marquardt and J. Majdalani, "Review of classical diffusion-limited regression rate models in hybrid rockets," *Aerosp.*, vol. 6, no. 6, p. 75, 2019.

[34] R. Bisin, A. Verga, D. Bruschi, and C. Paravan, "Strategies for paraffin-based fuels reinforcement: 3d printing and blending with polymers," in *AIAA Propul. Energy 2021 Forum*, (Virtual Event), pp. 1–20, 2021.

[35] L. J. Gibson and M. F. Ashby, "The mechanics of three-dimensional cellular materials," *Proc. R. Soc. Lond. A*, vol. 382, no. 1782, pp. 43–59, 1982.